GEOPHYSICS, VOL. 74, NO. 6 (NOVEMBER-DECEMBER 2009); P. WCA75–WCA81, 9 FIGS.
10.1190/1.3198210

Diffraction imaging by multifocusing

Alex Berkovitch[1], Igor Belfer[1], Yehuda Hassin[1], and Evgeny Landa[2]

ABSTRACT

Correct identification of geologic discontinuities, such as faults, pinch-outs, and small-size scattering objects, is a primary challenge of the seismic method. Seismic response from these objects is encoded in diffractions. Our method images local heterogeneities of the subsurface using diffracted seismic events. The method is based on coherent summation of diffracted waves arising in media that include interface discontinuities and local velocity heterogeneities. This is done using a correlation procedure that coherently focuses diffraction energy on a seismic section by flattening diffraction events using a new local-time-correction formula to parameterize diffraction traveltime curves. This time correction, which is based on the multifocusing method, depends on two parameters: the emergent angle and the radius of curvature of the diffracted wavefront. These parameters are estimated directly from prestack seismic traces. The diffraction multifocusing stack (DMFS) can separate diffracted and reflected energy on a stacked section by focusing diffractions to the diffraction location and defocusing the reflection energy over a large area.

INTRODUCTION

The localization of scattering objects such as faults, pinch-outs, sharp changes in reflectivity, and salt flanks is an important challenge in seismic exploration. The wavefields arising from such objects are characterized by the presence of scattered or diffracted energy. *Diffracted wave* means an edge diffraction, *scattered wave* means a scattering from objects or velocity perturbations of about the finite size of the Fresnel radius (Landa and Keydar, 1998). The curved elements of reflection interfaces also are sources of scattered energy. The kinematic characteristics of waves scattered from such elements are similar to those of waves from an edge (Klem-Musatov and Aizenberg, 1984; Klem-Musatov, 1994).

The energy of diffracted waves usually is weaker than that of specular reflections. Diffractions essentially are lost during the conventional processing/migration sequence, or they are masked in conventional seismic stacked sections. Local structural and lithological elements in the subsurface of a size comparable to the wavelength usually are ignored during processing and identified only during interpretation. Conventional common-midpoint (CMP) moveout corrections do not approximate diffraction traveltimes accurately; in addition, the CMP fold often cannot detect weak diffraction events. The summation of many traces is necessary for their detection. CMP acquisition often does not provide the necessary signal-to-noise ratio (S/N) for diffraction waves from sharp faults. As a result, migration cannot yield a proper image of such faults. Frequently, geophysicists confuse diffractions with triplications of reflection arrivals from curvilinear interfaces. True diffraction waves are attenuated very quickly (Klem-Musatov, 1994) with increasing distance from the apex.

The correct identification and use of diffraction events can be important for velocity estimation and interpretation (Reshef and Landa, 2009). Several attempts have been made to detect diffracted waves and use them for seismic interpretation. Efforts to image diffraction events are undertaken in Landa et al. (1987), Kanasewich and Phadke (1988), Landa and Keydar (1998), and Fomel et al. (2007). A methodology for identifying local targets in the shallow subsurface using refraction and diffraction waves is developed in Belfer et al. (1998). The separation of diffracted and reflected wavefields based on different focusing geometries is proposed in the focusing-defocusing approach of Khaidukov et al. (2004). That approach consists of focusing the reflection wavefield at imaginary sources (i.e., points where focusing of the reflection would occur at the instant time $t = 0$), muting areas of concentrated energy, defocusing the residual energy, and migrating the residual (diffracted) wavefield.

Another separation method for prestack data is described by Taner et al. (2006). They show that plane-wave decomposition naturally separates specular and diffracted events and allows the use of a plane-wave destruction filter to suppress specular events, resulting in plane-wave sections of diffractions. An approach to diffraction

Manuscript received by the Editor 21 January 2009; revised manuscript received 4 May 2009; published online 15 December 2009.
[1]Geomage Ltd., Modiin, Israel. E-mail: alex@geomage.com; igor@geomage.com; yehuda@geomage.com.
[2]Organisma Pétrolier de Recherche Appliquée (OPERA), Pau, France. E-mail: evgeny.landa@univ-pau.fr.

imaging in the depth-migrated domain is suggested by Moser (2008).

All of the methods mentioned above use the attenuation of the specular reflection and consider the residual wavefield as the diffraction part of the total wavefield. In this paper, we present a method based on an optimal summation of the diffracted events and the creation of an image containing mostly diffraction energy. This is enabled by a new time correction that accurately describes the moveout for diffraction events: a multifocusing moveout correction that uses a special condition valid for scattering events. Here, we describe the theory of the multifocusing method and demonstrate the efficiency of the proposed diffraction imaging technique on synthetic and field data.

MULTIFOCUSING METHOD

Multifocusing, a method for time imaging proposed by Berkovitch et al. (1994) and described by Berkovitch et al. (1998), Landa (2007), and Berkovitch et al. (2008), constructs a zero-offset section wherein each trace is computed from prestack traces located arbitrarily around an imaging position. The moveout correction does not require knowledge about the subsurface and is valid for arbitrary observation geometry. For a given source-receiver pair, the multifocusing moveout equations express the time shifts with respect to a zero-offset trace in terms of three parameters (for 2D problems): the emergent angle β of a normal ray (ray perpendicular to a reflector) and the curvature radii (R_{CRE} and R_{CEE}) of two fundamental circular wavefronts (Figure 1). The first wavefront (CRE, or common-reflection element) pertains to a source located where the zero-offset ray emitted from the central point X_0 hits the reflector (point O in Figure 1). The second wavefront (CEE, or common-evolute element) is formed by normal rays emitted from different points on the reflector (such as in an exploding reflector scenario).

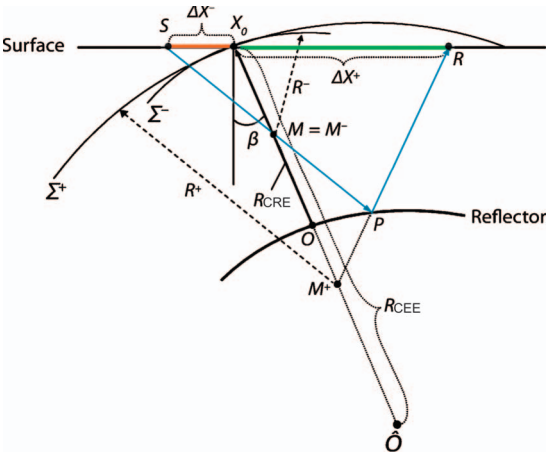

Figure 1. Scheme for the multifocusing ray diagram for a circular-arc reflector: M^- and M^+ are foci of fictitious wavefronts Σ^- and Σ^+; S and R are source and receiver positions; X_0 is the central-point coordinate (generally coincides with the CMP); ΔX^- and ΔX^+ are offsets of S and R from the central point; R^- and R^+ are the radii of curvature of the fictitious wavefronts; β is the incident angle for the normal-incidence ray; R_{CRE} and R_{CEE} are the radii of curvature of two fundamental wavefronts; and $\hat{O}$ is the curvature center (the evolute).

The center of curvature of this wavefront is situated on a caustic curve (Gelchinsky, 1992; Gelchinsky et al., 1999) called the *evolute*. In the case of a circular-arc reflector and constant overburden velocity, R_{CRE} is the distance between point O and the central point X_0. The caustic of the wavefront shrinks to a point $\hat{O}$ (evolute). The radius R_{CEE} in this case is the distance between point $\hat{O}$ and point X_0, which we call the central point.

Consider a normal ray that starts at point X_0 with the angle β to the vertical line (Figure 1). The ray hits the reflector at point O at normal incidence and returns to X_0. A ray from an arbitrarily located source S intersects the central ray at point M and is reflected back to the surface at receiver point R (a paraxial ray). The moveout correction for the arbitrary source and receiver offsets in the vicinity of the normal ray and for a laterally homogeneous macrovelocity model is described in the following equations (Berkovich et al., 2008):

$$\Delta\tau = \frac{\sqrt{(R^+)^2 - 2R^+\Delta X^+ \sin\beta + (\Delta X^+)^2} - R^+}{V_0} + \frac{\sqrt{(R^-)^2 + 2R^-\Delta X^- \sin\beta + (\Delta X^-)^2} - R^-}{V_0}, \tag{1}$$

where

$$R^+ = \frac{1+\sigma}{\frac{1}{R_{CEE}} + \frac{\sigma}{R_{CRE}}}, \quad R^- = \frac{1-\sigma}{\frac{1}{R_{CEE}} - \frac{\sigma}{R_{CRE}}}, \tag{2}$$

$$\sigma = \frac{\Delta X^+ - \Delta X^-}{\Delta X^+ + \Delta X^- + 2\frac{\Delta X^+ \Delta X^-}{R_{CRE}} \sin\beta}. \tag{3}$$

In these equations, ΔX^+ and ΔX^- are the source and receiver offsets for a given ray with respect to the central point X_0, R^+ and R^- are the radii of curvature of the fictitious waves defined by equations 2 and 3, V_0 is the near-surface velocity, which is assumed constant near the central point, and σ is a focusing parameter, the meaning of which will be clear later.

The double-square-root moveout equation 1 can be understood by considering a homogeneous medium with the velocity equal to the near-surface velocity V_0 (a priori data or iteration algorithms for estimation of V_0 variations are required if the medium is not homogeneous). In such a medium, the central and paraxial rays are combinations of straight-line segments. The first term on the right side of moveout correction 1 corresponds to the time along ray segment SM, which can be obtained from triangle SMX_0. The second term corresponds to the time along ray MPR and can be obtained from a similar consideration involving the imaginary source M^+ (image of the focusing point $M = M^+$). Point M^+ is the center of curvature for the fictitious circular wavefront Σ^+ just as $M = M^-$ is the center of curvature for the wavefront Σ^-.

Quantities R^+ and R^- involved in moveout correction 1 are radii of curvature of the fictitious wavefronts Σ^+ and Σ^-. As seen in Figure 1 for a given central ray, the radii R^+ and R^- depend upon the position of point M where the paraxial ray intersects the central ray and thus upon the position of the source and receiver that define the paraxial ray. Equations 2 for radii of curvature and equation 3 for the focusing parameter give the radii of curvature of the fictitious wave-

fronts R^+ and R^- in terms of the fundamental radii of curvature R_{CRE} and R_{CEE}, which are defined solely by the central ray only and are the same for all the source-receiver pairs in the vicinity of the central ray.

The dependence of radii R^+ and R^- on the position of the source and receiver (or on the position of M on the central ray) is contained in equation 3 for the focusing parameter, which has physical interpretation. In particular, $\sigma = 0$ means that $R^+ = R^- = R_{CEE}$, which implies that point M coincides with the center of curvature of the normal wavefront (or of the reflector) and corresponds to the case of a coinciding source and receiver (zero-offset configuration). For $\sigma = 1$ and $\sigma = -1$, radii $R^- = 0$ and $R^+ = 0$, corresponding to common-source and common-receiver configurations, respectively. For $\sigma = \infty$, both R^+ and R^- equal R_{CRE}, the situation in which focusing point M coincides with point O (common-reflection point).

The sensitivity of our method to variations in near-surface velocity V_0 is comparable to that of other methods to statics errors, i.e., the multifocusing method is mildly sensitive to V_0 variations after statics correction.

An alternative approach to zero-offset time imaging for arbitrary source-receiver positions is the so-called common-reflection surface (CRS) stacking method, proposed by Müller et al. (1998). The CRS method differs from the multifocusing approximation in traveltime moveout. The stacking parameters proposed in this method, i.e., the radius of curvature of the normal-incident-point (NIP) wave (R_{NIP}) and the radius of curvature of the normal wave (R_N), are identical to parameters R_{CRE} and R_{CEE} in the multifocusing method. Landa and Moser (2009) compare the CRS and multifocusing methods and show that for strongly curved reflectors, multifocusing formula 1 is remarkably accurate, whereas the CRS method becomes increasingly inaccurate.

The multifocusing parameters provide valuable information that can help interpret time sections and assist in further processing. In particular, multifocusing parameters can be used to estimate the dip-independent root-mean-square (rms) velocity for time migration:

$$V_{rms}^2 = \frac{2R_{CRE}V_0}{t_0}. \tag{4}$$

Velocities defined by equation 4, however, must be recalculated (Hubral, 1977) for time migration by taking into account the emergent angles β observed in the multifocusing method.

Implementation of the method is based on a phase correlation of the signal on the observed seismic traces included in the supergathers (i.e., gathers of traces with source and receiver in the vicinity of central point X_0). The data for the specific time t_0 are moveout corrected along different double-square-root traveltime curves to find the curve closest to that of the signal. The unknown parameters β, R_{CRE}, and R_{CEE} are estimated using a procedure that consists of finding a set of parameters that maximizes the semblance function calculated for all seismic traces in the supergather in a time window along the traveltime curve defined by the multifocusing moveout correction (equation 1).

The semblance function is maximized using a nonlinear global optimization method. The automated procedure looks for the set of parameters that maximizes the coherence criterion, calculated for all seismic traces in the vicinity of the central point within the bounds of the multifocusing aperture (superbase). It is important to emphasize that three multifocusing parameters are searched simultaneously on prestack traces. Any compromise to search parameters separately using prestack and poststack data could lead to inaccuracies in parameter estimation and jittered character of stacked sections. A simple geometric interpretation of the diffraction moveout correction is given in Appendix A.

DIFFRACTION IMAGING BY MULTIFOCUSING

The coherent summation of a large number of traces covering many CMP gathers increases the stacking power and S/N. Typically, the number of traces in the multifocusing supergather exceeds the CMP fold by at least one order of magnitude, thus allowing imaging of weak seismic events that cannot be seen by conventional processing. Diffractions constitute one type of event that might carry important information. Detection and imaging of diffractions are considerably more sensitive to noise than reflections because diffraction events typically are weaker than reflections. The CMP fold is often insufficient to detect weak diffraction events.

The situation is different for the moveout correction in the multifocusing method. Consider a situation in which the reflection interface in Figure 1 shrinks to a diffraction point O. Then, points P and M^+ will coincide with point O, and $R_{CRE} = R_{CEE}$. Hence, from equation 2 for the radii of curvature, we have $R^+ = R_{CRE} = R^- = R_{CRE}$. Substituting these values into expression 1 for moveout correction, we obtain the formula for multifocusing moveout correction of diffracted waves,

$$\Delta\tau = \frac{\sqrt{(R_{CRE})^2 - 2R_{CRE}\Delta X^+ \sin\beta + (\Delta X^+)^2} - R_{CRE}}{V_0} + \frac{\sqrt{(R_{CRE})^2 + 2R_{CRE}\Delta X^- \sin\beta + (\Delta X^-)^2} - R_{CRE}}{V_0}, \tag{6}$$

which is similar to expression 1. The moveout correction $\Delta\tau$ for a diffraction wave, however, depends on only two parameters: R_{CRE} and β. This fact simplifies computations and increases processing speed.

The practical implementation of diffraction stacking is a special case of multifocusing implementation. For diffraction stacking, however, only two parameters need to be searched: R_{CRE} and β. They are estimated by maximizing the semblance function calculated for all seismic traces in the supergather. The result is a time section containing primarily optimally stacked diffraction events. Such sections contain important information for identifying local heterogeneities and discontinuities in the subsurface.

In the multifocusing method, the size of the summation aperture around the central point X_0 for reflected waves is defined by the equation (Hubral et al., 1993)

$$W = \frac{2}{\cos\beta}\sqrt{\frac{V_0 T}{2\left|\frac{1}{R_{CEE}} - \frac{1}{R_{CRE}}\right|}}, \tag{7}$$

where T is the period of the signal ($T = 1/f$, with f the dominant frequency).

For diffracted waves, $R_{CEE} = R_{CRE}$ and therefore $W = \infty$, so theoretically it is possible to use an aperture of any size. However, this is not justified in the presence of strongly varying geologic conditions in the subsurface and strong attenuation of the diffracted energy. Therefore, to construct the diffraction multifocusing stack (DMFS),

we choose an aperture (source and receiver distances from the central point X_0) based on a projected Fresnel zone.

EXAMPLES

Synthetic data

The model shown in Figure 2a consists of a constant-velocity layer (3000 m/s) above a horizontal reflector at a depth of 1250 m and a point diffractor located at a depth of 625 m within that layer. Each of the 700 common-shot gathers has 128 traces, with shot and receiver spacing of 25 m. Band-pass-filtered white Gaussian random noise (S/N = 2) was added to the signal. The zero-offset section is shown in Figure 2b. Four steps were performed: (1) conventional multifocusing processing using formula 1 without selecting the reflected and diffracted waves; (2) DMFS construction (moveout correction 6); (3) poststack Kirchhoff time migration of the multifocusing result; and (4) poststack Kirchhoff time migration of the diffraction multifocusing result.

Standard multifocusing processing has imaged reflected and diffracted events (Figure 3a). Multifocusing stacking has suppressed noise to a great extent. Detection and interpretation of the diffraction responses from scatterers can be difficult or impossible because of interference by numerous strong reflections. The DMFS computed for the data in Figure 2b, using moveout correction equation 6, is shown in Figure 3b. This stack contains only the diffraction event; the reflection has been suppressed by the directional summation. Such a stack of field data can be used to identify local heterogeneities in the subsurface and analyze poststack migration velocity (Landa, 2007). The latter is possible by using the focusing criterion for diffraction events, i.e., through analysis of the curvature of the diffractions. Of significance, velocity estimation can be done in the poststack domain, something that cannot be done using reflections. Poststack time migrations of the multifocusing stack and DMFS in Figure 3a and b, using velocities obtained from focusing analysis of the diffraction event, are shown in Figure 3c and d, respectively.

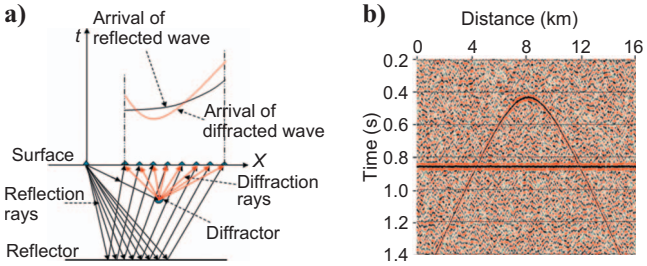

Figure 2. Common-shot gather for the synthetic data. (a) Ray scheme for a diffraction plus reflection model. (b) Minimum-offset gather. The diffractor is specified as a point scatterer. The reflector is horizontal.

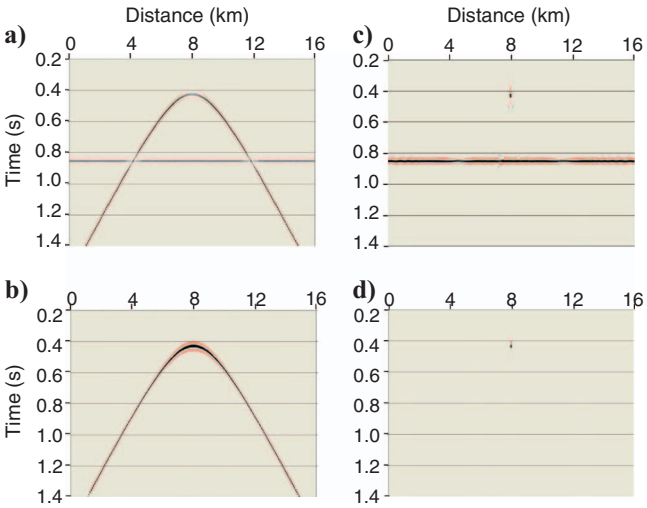

Figure 3. Processing result for the synthetic data: (a) multifocusing conventional stack, (b) DMFS, (c) Kirchhoff migration of the multifocusing conventional stack, and (d) Kirchhoff migration of the DMFS.

Field data

The next example treats 2D marine data from the offshore Mediterranean basin. The data set consists of 600 shot gathers with 25-m source and receiver spacing. Each shot record has 120 traces. To search for parameters in the conventional multifocusing analysis and moveout correction, we used the following ranges:

- β search: -0.45–0.45 radians with a 0.01-radian increment
- R_{CRE} search: 70–20,000 m with a 200-m increment
- R_{CEE} search: -1000–1000 m with a 10-m increment

Figure 4a shows the resulting multifocusing stacked section. According to geologic interpretation, a drawdown block between two subvertical faults is present between 1 and 5 km in the left part of the section (see the salt formation image marked by vertical green arrows). The pattern of reflections from the roof of a salt formation is well repeated in the dropped block. Diffraction events that occur along the top of the salt layer testify to its fractured structure. Summation in the multifocusing method also allows us to see some diffractions in the right part of the section (15.5 km). Figure 4b shows the DMFS. The reflection events are strongly attenuated, leaving well-imaged diffraction events from the roof of the salt as well as diffractions from the subvertical faults. Diffractions toward the right side of the section (15.5 km) suggest subtle faulting. The presence

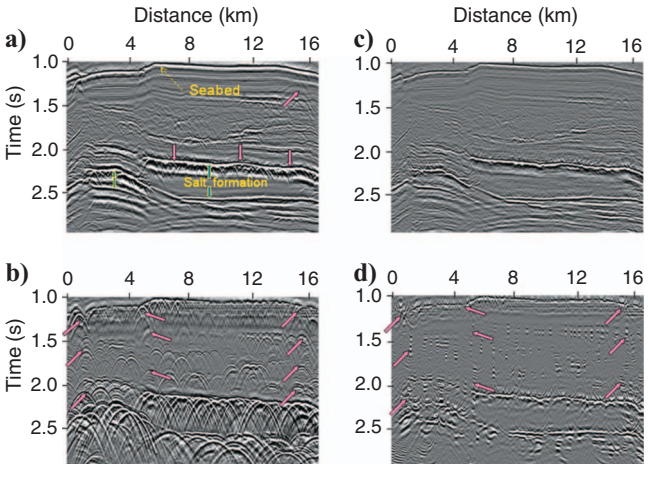

Figure 4. Processing result for field marine data (Mediterranean basin): (a) multifocusing conventional stack, (b) DMFS, (c) Kirchhoff migration of the multifocusing conventional stack, and (d) Kirchhoff migration of the DMFS. Pink arrows point to assumed fault positions; green arrows point to the salt formation interval.

of diffractions also indicates seabed roughness. Nonspecular reflections from the top of salt exist in the Kirchhoff migration of multifocusing stack (Figure 4c). However, the faults in the left part of this section and moreover in the right part are hardly evident.

Localized diffracting objects that gave rise to the diffractions in Figure 4c are seen in sharp relief on the migrated diffraction multifocusing stack (Figure 4d). The amplitudes of these objects are shown in color on the multifocusing stack in Figure 5. All faults, including subtle ones, are traced. The interesting feature is the nonspecular nature of the reflection from the salt roof at about 2.2 s, starting at about 6 km and extending to the right side of the figure. Undoubtedly, this reflection takes into account a velocity step between salt formations and capping strata. However, surface irregularities create an additional diffraction field.

Also of interest is the appearance of overmigration (i.e., smiles) for many localized features connected with the salt formation. This suggests that the migration velocities could be refined to lower values and that the migrated DMFS can be used to refine estimates of velocity beyond those computed from the DMFS. Although the imaged diffractions show features that are highly localized laterally, they extend vertically (in time) because of the finite bandwidth of the data. The local objects in the time interval 1.0–2.0 s and below the base of the salt formation, which gave rise to the strong diffraction events in the diffraction multifocusing stack (Figure 4b), are well localized in the migration result. In this way, the diffraction multifocusing stack can help in the interpretation of seismic data.

It is interesting to compare the velocity model (rms velocities obtained from the measured radius R_{CRE} via equation 4, computed using the standard multifocusing algorithm; Figure 6a) with velocities calculated by selecting optimal values in DMFS migration (Figure 6b). The resolution of the velocity field clearly has increased. The corrected velocities (Figure 6b) are more consistent with the geologic concept of a dropped block between distances of 1 and 5 km. Velocities for DMFS migration are determined by focusing the diffraction events during migration of the multifocusing DMFS. In practice, we operate with several different velocities and then pick the one that focuses best. The velocity field after choosing optimal values shows distinctly more lateral variations than the original field did, which means the diffraction velocity field has better resolution.

The goal of the processing is to build not only a detailed seismic section but also a velocity model that provides accurate poststack and prestack depth imaging, displaying the layered structure as well as other local objects that will assist in the interpretation process. A flowchart for the multifocusing diffraction processing and interpretation shown in Figure 7 can be proposed.

According to the flowchart, the processing starts along two parallel paths. One begins from construction of the conventional multifocusing stack, and the other begins from construction of the DMFS. The initial velocity model for subsequent imaging is provided from parameters obtained while building the conventional multifocusing stack. This model, however, lacks the localized information to migrate the multifocusing stack properly. The strategy for updating the velocity model is realized by analyzing the DMFS. Specifically, the rms velocity can be obtained from focusing analysis of the diffraction events that are well imaged in the DMFS. Practically, it is performed by testing the constant velocities and focusing of diffraction arrivals with migration. Thus, the focusing of diffraction events yields the refined velocity model. Then the migrated images of the multifocusing stack and the diffraction-enhanced stack are used for joint geologic interpretation.

This processing approach can be included in any modern 2D or 3D multifold data processing system to detect local objects, to correct velocity models, and to provide an additional means for interpreting data acquired where subsurface geology is complex. The 3D implementation of the DMFS in general requires evaluation of five multifocusing parameters (two angles and three radii). Clearly, a high-performance computing system is needed for this purpose.

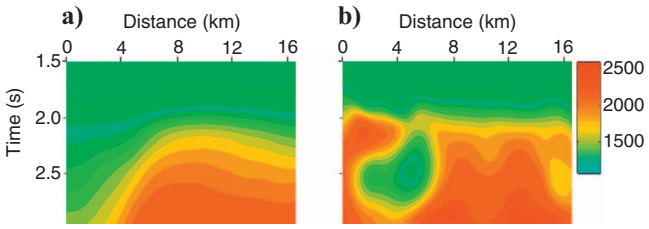

Figure 6. The rms velocities from processing the field data (Figure 4). (a) Smoothed velocity field obtained from multifocusing conventional stacking. (b) Corrected velocity field obtained with interactive procedure performed by DMFS (migration).

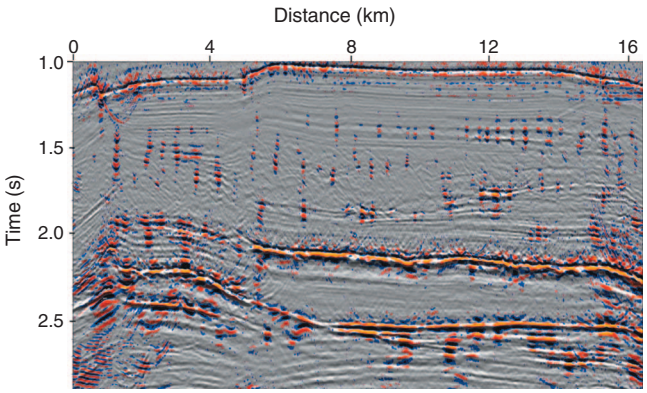

Figure 5. Diffraction points from Figure 4d superimposed on the image of Figure 4c.

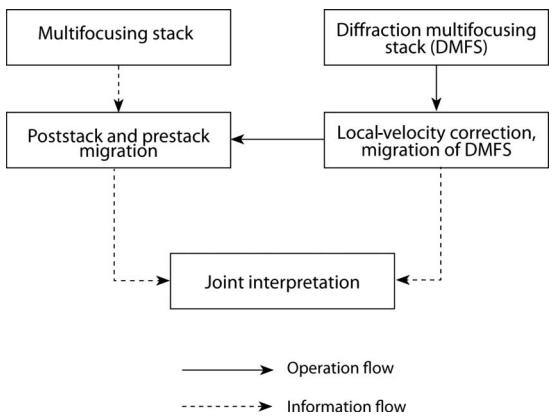

Figure 7. Flowchart describing the procedure of DMFS construction, velocity analysis, and interpretation.

DISCUSSION

Interest in diffraction events has increased since 1999. Diffractions play an important role in seismic data processing and interpretation: they are direct indicators of localized heterogeneities in the subsurface and carriers of potentially accurate and high-resolution information about subsurface velocities. So, why until now have diffractions not been exploited widely for these purposes? The answer, in our opinion, is that diffractions have weak energy, they are masked by strong reflections, and processing and imaging algorithms and procedures are not optimal to detect diffraction events. Conventional CMP stacking tends to filter out diffractions (or it does not stack them optimally). Poststack migration algorithms purport to focus diffraction energy but typically operate on data in which diffraction energy has been suppressed by the CMP stack. Of course, this is not the case for prestack time migration, but these require an accurate velocity model — a problem in itself.

Multifocusing processing opens the possibility of enhancing diffraction events and estimating their parameters, such as wavefront curvature and emergent angles. This becomes possible because of a time-correction formula that is optimal for reflection and diffraction events, in contrast to conventional CMP parameterization which is optimal for reflection events only. In this parameterization, moveout correction for seismic events is described by the double-square-root equation with three parameters: an emergent angle and two radii of curvature of the two fundamental wavefronts. The diffractor can be considered as a point reflector; then the two wavefronts with radii R_{CRE} and R_{CEE} coincide. This condition of coinciding R_{CRE} and R_{CEE} constitutes the essence of our algorithm for diffraction imaging. In practice, this means that instead of searching three parameters for multifocusing moveout correction 1, we search for two parameters using moveout expression 6. As a consequence, diffraction events are stacked coherently, whereas reflections undergo nonoptimal summation and thus are suppressed.

Diffraction is essentially a 3D phenomenon. Unlike reflection, diffraction energy is emitted in all directions from a scattering object and has no dominant propagation direction. Thus, it is important to develop a 3D diffraction-imaging algorithm. In theory, this can be done relatively simply by describing the traveltime correction surface in terms of the emergent angles in two orthogonal directions (x and y) and three radii of wavefront curvature ($R_{x\mathrm{CRE}}$ in the x-direction, $R_{y\mathrm{CRE}}$ in the y-direction, and $R_{xy\mathrm{CRE}}$ for mixed radius). Ideally, this would mean searching for five unknown parameters.

Even using modern cluster technologies, this task is computationally intensive, suggesting the need for compromises. One such compromise is to assume that the diffraction wavefront can be approximated adequately by a sphere in the vicinity of the imaging point. Then $R_{x\mathrm{CRE}} = R_{y\mathrm{CRE}}$ and $R_{xy\mathrm{CRE}} = 0$ and three-parameter search is sufficient. Such an approximation is acceptable for media with moderate lateral variation and relatively small summation apertures.

CONCLUSIONS

We have proposed a new technique for detecting local subsurface heterogeneities using diffraction multifocusing stack. The imaging is based on a new type of local time correction for diffraction traveltime curve parameterization. This correction is valid for arbitrary subsurface models and for arbitrary source-receiver configurations. The DMFS method consists of optimal stacking of seismic data along actual diffraction traveltime curves. The stacking procedure produces a section in which diffractions are emphasized and specular reflections are illuminated. The diffraction multifocusing stacks can be used for reliable interpretation of nonsmoothed geologic interfaces and for identification of local heterogeneities such as faults, karsts, and fractures. In addition, the diffraction stack can be useful for refining time migration velocity by focusing analysis of diffraction events. Application of the method on synthetic and real data demonstrates efficiency and reliability of the proposed procedure.

ACKNOWLEDGMENTS

We gratefully acknowledge the careful corrections, comments, and suggestions of Ken Larner. We also are thankful to the associate editor (Isabelle Lecomte) and three anonymous reviewers for many helpful suggestions and improvements. One of the authors (E. Landa) thanks TOTAL for supporting this research. OPERA is a private organization funded by TOTAL and affiliated with Pau University.

APPENDIX A

MOVEOUT CORRECTION FOR DIFFRACTED WAVES

Our goal here is to determine the time shift for any shot and receiver in the multifocusing supergather near the central point X_0 (Figure A-1). The energy of a diffracted wave spreads from the point of diffraction in all directions (Klem-Musatov, 1994) as shown in Figure A-2b, unlike the reflected wave, whose exit point at the surface is dependent on the shot position and reflector shape (Figure A-2a). According to Figure A-1, the moveout correction for normal ray OX_0 for the trace corresponding to shot S and receiver R is given by

$$\Delta t = \frac{L_{SO} + L_{OR}}{V_0} - \frac{2R_{\mathrm{CRE}}}{V_0}, \qquad \text{(A-1)}$$

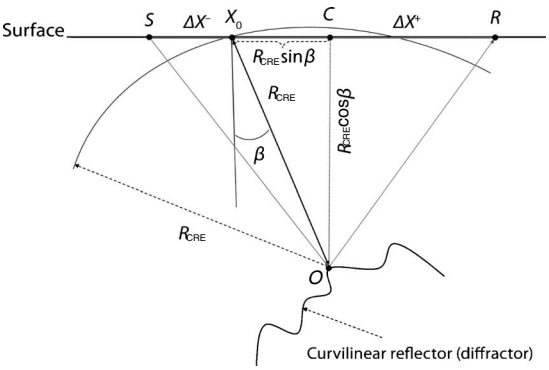

Figure A-1. Multifocusing ray diagram for diffracted wave detection: O is a diffraction point; C is the vertical projection of the diffraction point on the surface; X_0 is the central point; S and R are the source and receiver positions; ΔX^- and ΔX^+ are offsets of S and R from the central point; β is the incident angle; and R_{CRE} is the radius of curvature of the fundamental (diffraction) wavefront.

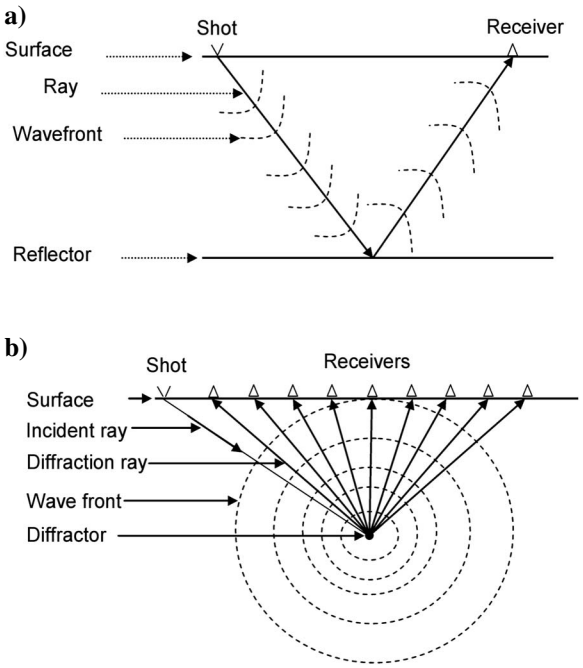

Figure A-2. Ray schemes for (a) reflected and (b) diffracted waves.

where

$$L_{SO} = \sqrt{(\Delta X^- + R_{\mathrm{CRE}} \sin\beta)^2 + (R_{\mathrm{CRE}} \cos\beta)^2} = \sqrt{R_{\mathrm{CRE}}^2 + 2\Delta X^- R_{\mathrm{CRE}} \sin\beta + (\Delta X^-)^2}$$

and

$$L_{OR} = \sqrt{(\Delta X^+ - R_{\mathrm{CRE}} \sin\beta)^2 + (R_{\mathrm{CRE}} \cos\beta)^2} = \sqrt{R_{\mathrm{CRE}}^2 - 2\Delta X^+ R_{\mathrm{CRE}} \sin\beta + (\Delta X^+)^2}. \quad \text{(A-2)}$$

Then

$$\Delta\tau = \frac{\sqrt{(R_{\mathrm{CRE}})^2 - 2R_{\mathrm{CRE}}\Delta X^+ \sin\beta_0 + (\Delta X^+)^2} - R_{\mathrm{CRE}}}{V_0} + \frac{\sqrt{(R_{\mathrm{CRE}})^2 + 2R_{\mathrm{CRE}}\Delta X^- \sin\beta_0 + (\Delta X^-)^2} - R_{\mathrm{CRE}}}{V_0}. \quad \text{(A-3)}$$

REFERENCES

Belfer, I., I. Bruner, S. Keydar, A. Kravtsov, and E. Landa, 1998, Detection of shallow objects using refracted and diffracted seismic waves: Applied Geophysics, **38**, 155–168.

Berkovitch, A., I. Belfer, and E. Landa, 2008, Multifocusing as a method of improving subsurface imaging: The Leading Edge, **27**, 250–256.

Berkovitch, A., B. Gelchinsky, and S. Keydar, 1994, Basic formulae for multifocusing stack: 56th Meeting, EAEG, Expanded Abstracts, 140.

Berkovitch, A., S. Keydar, E. Landa, and P. Trachtman, 1998, Multifocusing in practice: 68th Annual International Meeting, SEG, Expanded Abstracts, 1748–1751.

Fomel, S., E. Landa, and T. Taner, 2007, Poststack velocity analysis by separation and imaging of seismic diffractions: Geophysics, **72**, U89–U94.

Gelchinsky, B., 1992, Homeomorphical imaging method of analyzing the structure of a medium: U. S. Patent 5 103 429.

Gelchinsky, B., A. Berkovitch, and S. Keydar, 1999, Multifocusing homeomorphic imaging: Part 1 — Basic concepts and formulas: Applied Geophysics, **42**, 229–242.

Hubral, P., 1977, Time migration — Some ray theoretical aspects: Geophysical Prospecting, **25**, 738–745.

Hubral, P., J. Schleicher, M. Tygel, and C. Hanitzsch, 1993, Determination of Fresnel zones from traveltime measurements: Geophysics, **58**, 703–712.

Kanasewich, E., and S. Phadke, 1988, Imaging discontinuities on seismic sections: Geophysics, **53**, 334–345.

Khaidukov, V., E. Landa, and T. Moser, 2004, Diffraction imaging by focusing-defocusing: An outlook on seismic superresolution: Geophysics, **69**, 1478–1490.

Klem-Musatov, K., 1994. Theory of seismic diffractions: SEG.

Klem-Musatov, K. D., and A. M. Aizenberg, 1984, The ray method and the theory of edge waves: Geophysical Journal of the Royal Astronomical Society, **79**, 35–50.

Landa, E., 2007, Beyond conventional seismic imaging: EAGE.

Landa, E., and S. Keydar, 1998, Seismic monitoring of diffraction images for detection of local heterogeneities: Geophysics, **63**, 1093–1100.

Landa, E., and T. J. Moser, 2009, Multifocusing revisited — Inhomogeneous media and curved interfaces: 71st Conference & Exhibition, EAEG, Expanded Abstracts, U026.

Landa, E., V. Shtivelman, and B. Gelchinsky, 1987, A method for detection of diffracted waves on common-offset sections: Geophysical Prospecting, **35**, 359–373.

Moser, T., 2008, Diffraction imaging in depth: Geophysical Prospecting, **56**, 627–641.

Müller, T., R. Jäger, and G. Höcht, 1998, Common reflection surface stacking method — Imaging with an unknown velocity model: 68th Annual International Meeting, SEG, Expanded Abstracts, 1764–1767.

Reshef, M., and E. Landa, 2009, Poststack velocity analysis in the dip-angle domain using diffractions: 70th Conference & Exhibition, EAGE, Extended Abstracts.

Taner, T., S. Fomel, and E. Landa, 2006, Separation and imaging of seismic diffractions using plane-wave decomposition: 76th Annual International Meeting, SEG, Expanded Abstracts, 2401–2405.